

# Embedded System for Responsive Optogenetic Control of Spontaneous Seizures in a Preclinical Temporal Lobe Epilepsy Model

Sofie Lasure<sup>1,2</sup><sup>a</sup>, Lien De Schaepmeester<sup>2</sup><sup>b</sup>, Sielke Caestecker<sup>2</sup><sup>c</sup>, Jeroen Spanoghe<sup>2</sup><sup>d</sup>,  
Marijke Vergaelen<sup>2</sup><sup>e</sup>, Rik Verplancke<sup>1</sup><sup>f</sup>, Johannes Vierock<sup>3</sup><sup>g</sup>, Robrecht Raedt<sup>2</sup><sup>h</sup> and  
Pieter Bauwens<sup>1</sup><sup>i</sup>

<sup>1</sup>Center for Microsystems Technology, Imec and Ghent University, Belgium

<sup>2</sup>4BRAIN, Department of Head and Skin, Ghent University, Belgium

<sup>3</sup>Neuroscience Research Center, Charité, Universitätsmedizin zu Berlin, Germany  
fi

**Keywords:** Epilepsy, Responsive Neuromodulation, Optogenetics, MSP430 Microcontroller, Embedded System.

**Abstract:** **Aims:** Responsive neuromodulation employing optogenetics is a promising therapy which provides spatial and temporal specificity for temporal lobe epilepsy (TLE), a neurological disorder characterised by the occurrence of spontaneous seizures. In this study, we evaluated whether seizures could be detected with a self-designed minimalist embedded system and terminated through activation of the WiChR opsin in the intrahippocampal kainic acid (IHKA) mouse model of temporal lobe epilepsy. **Methods:** Mice were injected in the hippocampus with kainic acid to simulate TLE and with the AAV2/9 viral vector to induce expression of the WiChR opsin. Intracranial EEG was recorded and processed with a low-power microcontroller to detect the seizure via the amplitude correlation metric. Upon detection, a 473 nm Light Emitting Diode (LED) was activated to illuminate the hippocampus through an optrode. **Results:** It was possible to responsively illuminate seizures with the embedded system and achieve a significant reduction in seizure duration with a pulse train of 10 Hz, 5 ms, 10 mW for 90 s. A brief parameter study was performed although preliminary results were inconclusive. **Conclusions:** In this study, we prove that we can responsively suppress seizures in the IHKA mouse model within the limitations of a minimalist embedded system. Additionally, the WiChR opsin has been demonstrated to have a high potential for efficient seizure suppression with limited illumination.

## 1 INTRODUCTION

Temporal lobe epilepsy (TLE) is a chronic neurological condition characterised by recurrent seizures originating in the temporal lobe of the brain. While the use of anti-seizure medication remains the first line of treatment, neuromodulation offers a promising alternative for patients whose seizures are not adequately controlled by medication or for whom resective surgery is not an option. Neuromodulation

is a technique where the brain is stimulated, usually electrically, and has been proven a viable therapy for several neurological disorders, including TLE. Both Deep Brain Stimulation (DBS) and the Responsive Neuromodulation System (RNS) have been FDA-approved and have shown promise in reducing seizure frequency and improving quality of life for patients (Ryvlin and Jehi, 2021; Ebrahim and Tungu, 2022).

However, there remain significant drawbacks to the use of electrical stimulation. The electrical pulses affect a large area of the brain, including neurons and neuronal projections not related to the neurological disorder. Optical stimulation can provide a solution as the stimulated area is much smaller, allowing stimulation with an increased spatial specificity. Optical stimulation would have a limited effect on the brain activity so it must be used in combination with techniques like optogenetics or optopharmacology (Ebrahim and Tungu, 2022).

With optogenetics, light sensitive proteins

<sup>a</sup> <https://orcid.org/0000-0001-8625-5896>

<sup>b</sup> <https://orcid.org/0009-0000-6660-0541>

<sup>c</sup> <https://orcid.org/0000-0001-7398-183X>

<sup>d</sup> <https://orcid.org/0000-0002-4427-0948>

<sup>e</sup> <https://orcid.org/0000-0002-2915-667X>

<sup>f</sup> <https://orcid.org/0000-0002-6642-9454>

<sup>g</sup> <https://orcid.org/0000-0001-7368-5539>

<sup>h</sup> <https://orcid.org/0000-0002-8939-0169>

<sup>i</sup> <https://orcid.org/0000-0001-9398-2485>

(opsins) are introduced through the use of a viral vector. These opsins can be activated by illumination, either exciting or inhibiting a cell's activity (Medina et al., 2023). The WiChR opsin is a novel inhibitory channelrhodopsin that introduces light-sensitive potassium ion channels, maximally activated by light pulses with a wavelength around 470 nm. Compared to other opsins, the WiChR opsin has some major advantages as the potassium ion channels have a larger photocurrent during illumination and the opsins close relatively slowly, allowing for efficient (Vierock et al., 2022).

Optopharmacology uses light-sensitive compounds which can be locally activated with optical stimulation. An example of this type of compound is photocaged N6-cyclopentyladenosine (cCPA) which can be activated by 405 nm illumination (Craey et al., 2022; Spanoghe et al., 2024). A novel epilepsy treatment is under development using optopharmacology in combination with the use of evoked potentials (EP's), which are neuronal responses to a stimulation pulse and are linked to the excitability of the brain. Controlling the excitability, as extracted from the EP's, using responsive activation of cCPA has been shown to reduce the occurrence of seizures *ex vivo* (Craey, 2022).

The final goal when developing responsive neuromodulation therapies is twofold: (1) a proof-of-concept of the therapeutic effect and (2) the ability to run these therapies on an implantable device. Both goals present their own unique challenges but are inherently linked to each other through the required hard- and software. The aim of the development of this embedded system was focused towards an implantable device but adjusted to allow neuromodulation experiments within a preclinical setting. Therefore, there were two main design considerations: (1) implementation within an existing EEG recording set-up and (2) the possibility for miniaturisation to allow development towards an implantable device.

This paper will describe the design of hard- and software of this embedded system. This device was used to conduct a feasibility study of a neuromodulation therapy where seizures were suppressed upon detection in the Intrahippocampal Kainic Acid (IHKA) mouse model of TLE using the novel WiChR opsin, illustrating that this is possible even with minimalist hard- and software (Zeidler et al., 2018). Within this experiment, an initial exploration of the stimulation parameter space was performed to increase the understanding of the behaviour of the WiChR opsin and search for the most efficient illumination protocol.

## 2 METHODS

### 2.1 Embedded System

A major design consideration in the development of this particular embedded system was the outlook for development towards a thin, flexible, implantable device. To facilitate this, the number of components had to be minimised and the components had to be available in the smallest packaging factor, i.e. as bare dies for the Integrated Circuits (IC's) which was a major limitation in component selection.

Additionally, to ensure a seamless interface within the existing recording set-up and allow usage as a more general purpose responsive neuromodulation system, both hard- and software were designed with ample connectors and possibilities to modify the system depending on a given experiment. The embedded system takes the amplified and filtered EEG signals as input and generates an output signal used to drive a stimulation system. The embedded system generates output signals which are recorded together with the EEG-signals to allow monitoring of the functioning of the responsive neuromodulation system and obtain a synchronised recording of both. The integration of the embedded system within the electrophysiology set-up is illustrated in Figure 1A.

#### 2.1.1 Hardware

The embedded system is based upon designs found in literature and designed around a low-power microcontroller unit (MCU) of the MSP430-family from Texas Instruments (Pederson et al., 2019; Shon et al., 2017). Besides the microcontroller and the required components for the programming circuitry, there are voltage regulators present which convert a single supply voltage into a double supply rail and generate 3.3 V as required by the MCU. Incoming signals pass through a voltage offset circuit of 1.65 V to offset the incoming signals and to ensure they are within the Analog-to-Digital Converter (ADC) input range, as shown in Figure 1B. On the output side, two Digital-to-Analog Converters (DAC's) are used. The first is used to transmit the metric used for the responsive neuromodulation to use as feedback on how the embedded system is performing. The second DAC is used to control the stimulation parameters. Using a switch, a choice can be made between voltage and current pulses. Voltage pulses are generated using a negative offset and an amplifier as shown in Figure 1C. These can be used for direct stimulation or used as a trigger for an external stimulation source, e.g. a laser or Light Emitting Diode (LED) driver.

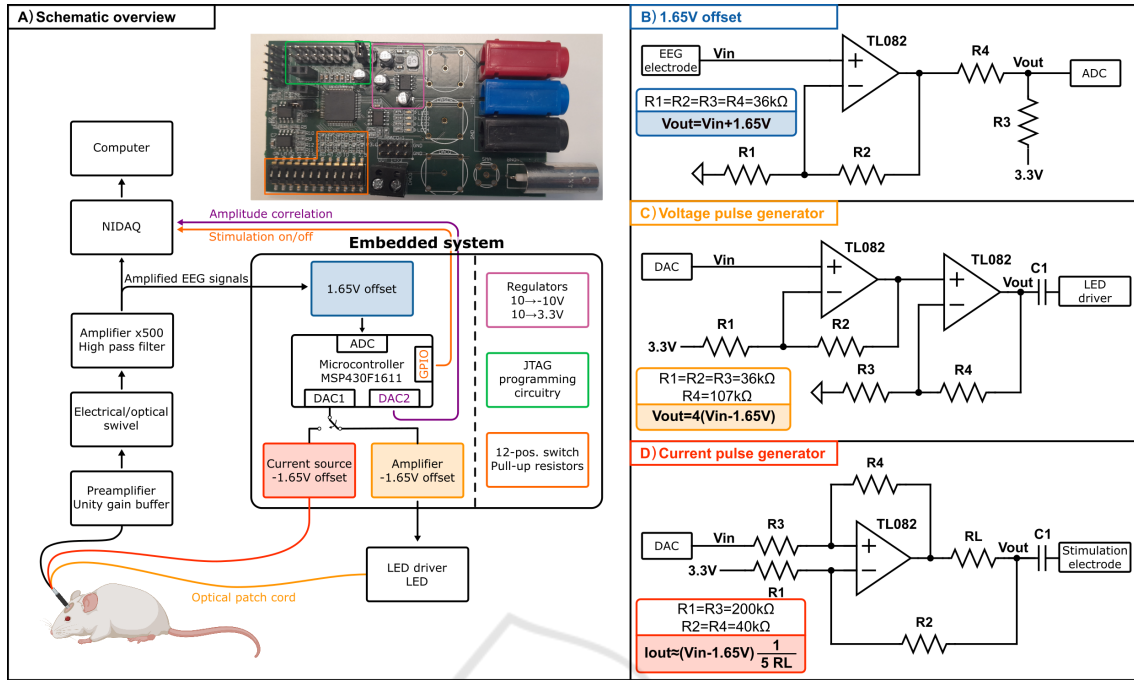


Figure 1: A: Schematic overview of electrophysiology set-up and integration of embedded system within. Build-up of embedded system and picture of realisation. NIDAQ: National Instruments Digital Acquisition Device. B: 1.65 V voltage offset circuit. C: Voltage pulse generator circuit including -1.65 V offset. D: Howland current source including -1.65 V offset.

Current pulses are generated using a Howland current source as shown in Figure 1D (Pederson et al., 2019; Instruments, 2008). The circuit delivers an output current as shown in Equation 1 where the second factor is negligible if the  $R_1/R_2 = R_3/R_4 = k$ . Using the resistor  $R_L$ , the maximal stimulation current can be dimensioned but a trade-off must be found between the range of the output current and the resistance of the stimulation electrode since they are related as shown in Equation 2. For a stimulation electrode resistance  $R_{electrode}$  of 10 k $\Omega$  and an opamp supply rail of 10 V, which results in an opamp output swing and thus  $V_{out}$  of 8 V, the output current will be limited to 800  $\mu$ A.  $V_{in}$  is limited to  $\pm 1.65$  V corresponding to the output of the MCU DAC after the -1.65 V offset which means  $R_L$  will be dimensioned at 825  $\Omega$  for  $R_1 = R_3 = 200$  k $\Omega$  and  $R_2 = R_4 = 40$  k $\Omega$ . When dimensioning for increasing resistances of the stimulation electrode,  $R_L$  will have to be increased and the maximal output current will decrease. Increasing the voltage supply rails can mitigate this trade-off (Instruments, 2008).

$$I_{out} = V_{in} \frac{1}{kR_L} + V_{out} \frac{\left(\frac{R_4}{R_3} - \frac{R_2}{R_1}\right)}{R_2} \quad (1)$$

$$\text{with } k = \frac{R_1}{R_2} = \frac{R_3}{R_4}$$

$$I_{out} = V_{in} \frac{1}{kR_L} = \frac{V_{out}}{R_{electrode}} \quad (2)$$

A pin header is used to connect an MSP MCU programming and debugging probe (MSP-FET, Texas Instruments, Texas, USA) to reprogram the MCU. Pin headers, as well as BNC-connectors can be used to connect incoming and outgoing signals

## 2.1.2 Seizure Detection Algorithm

Considering the computational limitations of the MSP430F1611 microcontroller, a relatively simple yet robust seizure detection algorithm is needed. Seizures in the IHKA mouse model are characterised by high frequency spiking activity observed in intracranial EEG-signals, which can be detected using peak detection. However, as this is computationally expensive, an alternative metric called Amplitude Correlation (AC) is used as described in literature (Krook-Magnuson et al., 2013; White et al., 2006).

The amplitude correlation metric is based upon the use of the signal range in a window with e.g. a length of 120ms. For each window, the overlap of the signal range is calculated with respect to those of the previous N windows. In other words, the amplitude correlation will only be high if the signal range in the current window is high and similar to the range in previous window(s), hence the term "correlation", which is illustrated in Figure 2 for a window size of 1 s. As seizures are characterised by a prolonged period ( $\geq 5$  s) of high frequency spiking (Zeidler et al.,

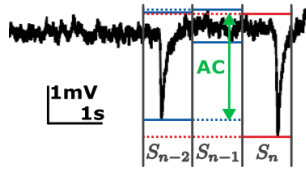


Figure 2: The amplitude correlation (AC) is calculated as the overlap of the signal range in current window  $S_n$  with the previous  $N$  windows, here illustrated for a window size of 1 s.

2018), a summation of the amplitude correlation is introduced to avoid a response to brief periods of spiking activity which would be considered a false positive. High frequency spiking activity for a prolonged period will increase the summed amplitude correlation and based on a threshold crossing, a seizure detection is initiated. Mathematically, this is expressed as the following formulas with  $S$  representing a window:

$$\text{Amplitude correlation } AC(S_n) = \min[\max(S_n), \max(\max(S_{n-1}), \max(S_{n-2}))] - \max[\min(S_n), \min(\min(S_{n-1}), \min(S_{n-2}))] \quad (3)$$

$$AC_{\text{summed},n} = \frac{1}{n_{\text{sum}}} \sum_{i=1}^{n_{\text{sum}}} AC_{n-i} \quad (4)$$

The amplitude correlation can be tuned by modifying (1) the window size, (2) the number of windows to calculate the amplitude correlation with and (3) the number of windows to consider in the summation. The window size and the number of windows used to calculate the amplitude correlation affect the minimal epileptic peak frequency needed for detection. With windows of 120 ms and 3 windows to consider as used by Krook-Magnuson et al., the spiking frequency has to be at least 5.5 Hz to have an impact on the amplitude correlation as seen in Equation 5 (Krook-Magnuson et al., 2013). In the IHKA mouse model, a minimum spiking frequency of 2 Hz is typically used to classify seizures (Zeidler et al., 2018) so the amplitude correlation settings are modified to use 6 windows instead of 3 (including the current window). Modifying the number of windows included in the summation affects the minimal required duration of spiking activity and is set to 42 to correspond to a period with spiking activity with a minimal duration of 5 s. With these settings, a seizure with repetitive spiking of 2 Hz will be detected within approximately 5 s and a seizure with a higher frequency will be detected faster in about 2 s as more windows will have a high AC.

$$\text{Spiking freq.} = \frac{2 \text{ spikes}}{3 \text{ windows} \cdot 120 \text{ ms}} = 5.5 \text{ Hz} \quad (5)$$

### 2.1.3 Software Implementation

The implementation of the previously described algorithm is relatively simple but becomes increasingly complex with the inclusion of various features to facilitate neuromodulation experiments as it must include the following options: (1) change the detection/stimulation parameters for each detection, (2) enable randomisation of sequence of various elements, (3) disable stimulation after a set amount of time, (4) re-enable stimulation with another set of elements and (5) the option to configure settings during an ongoing recording.

The incoming EEG-signals are recorded per window with a duration of 120ms, during which the current minimum and maximum are stored. Upon finishing the window, a flag is set to initiate the calculation of the amplitude correlation. If this is above the "up" threshold, an element is started, which can be either a detection or a stimulation element. A stimulation element consists of a pulse train with a certain amplitude, pulse duration, pulse frequency, stimulation duration as well as an additional flag which can be used for special settings, e.g. reduction of pulse duration after  $X$  seconds. An element is only considered as "finished" when the amplitude correlation drops below a "down" threshold to ensure a seizure is fully finished prior to starting a new element. The elements are defined within a parameter set which specifies the number of elements and their parameters. As the sequence of the elements could have a confounding effect on the results, the sequence is randomised before the execution of each series of elements. Finally, there is the option to customise parameters using a 12-position switch. The MCU periodically checks the settings of this switch and adjusts the parameters accordingly. The exact changes are experiment-dependent and pre-programmed prior to each experiment.

The software is written in C in Code Composer Studio (Texas Instruments, Dallas, Texas, USA) and programmed onto the microcontroller using the MSP-FET debugging probe (Texas Instruments, Dallas, Texas, USA). The structure of the software is based around a simple main-loop and extensive use of interrupts as most of the actions are time-dependent. Two timers are used, both derived from the Microcontroller Unit (MCU) clock. The first timer is configured with a higher clock frequency as it will control the timing of the ADC (sampling frequency 2kHz) and the stimulation pulses (switching speed up to 1 kHz). The second timer uses a lower clock frequency for the long term timing (range seconds-minutes) to control long-term changes between parameter sets. An ADC interrupt will control digitisation of the incoming signals. The maximum clock

frequency of the MCU is 4.9 MHz so allows for pulses down to 0.2  $\mu$ s which is sufficient for most stimulation protocols as optical stimulation usually employs pulses  $\geq 0.5$  ms and current pulses for evoked potentials use segments of 200  $\mu$ s.

## 2.2 Responsive Seizure Suppression in the IHKA Mouse Model

### 2.2.1 Surgical Interventions

All experiments were conducted with male C57Bl/6J mice (n=12, Janvier, The Netherlands) acquired at an age of 7 weeks. Animals were treated according to the European guidelines (directive 2010/63/EU). All experiments described in the following were approved by the Animal Experimental Ethical Committee of Ghent University (ECD 22-39) and complied with the ARRIVE guidelines. Mice were housed under environmentally controlled conditions (humidity: 40–60 %, temperature: 20–23 °C), a controlled 12 h/12 h light/dark cycle and with ad libitum access to food and water.

For the injections and implantations, the animals were secured in a stereotactic frame (Neurostar Robot Stereotaxic system, Neurostar, Tübingen, Germany) using ear bars and brought under anaesthesia, isoflurane (induction 5 %, maintenance 2 %) and medical O<sub>2</sub> (induction 1 l/min, maintenance 0.8 l/min). Injection of 50 nl kainic acid (200 ng kainic acid in 50 nl saline) was done to induce status epilepticus with a flow rate of 250 nl/min (Nanoliter 2020, WPI, Florida, United States) at the stereotactic coordinates AP-2.0 mm relative to bregma; ML+1.5 mm relative to bregma; DV-1.8 mm relative to dura (Desloovere et al., 2021). Three weeks thereafter, 1000 nl of the pAAV2/9.hsyn-WiChR1-ts-mScarlet-er-WPREneu viral vector (titer 8.47E+12 VG/ml) was injected with a flow rate of 100 nl/min at the same location. After 2 weeks, the optrode was implanted at the same location with a depth of DV-1.8 mm relative to dura. The optrode consisted of a bipolar depth electrode formed by twisting polyimide-coated stainless steel wires ( $\phi$ 70  $\mu$ m, California Fine Wire, USA) and assembling these with an implantable optical fibre ( $\phi$ 400  $\mu$ m, length 5 mm, 1.25 mm ferrule, CFMLC14L05, Thorlabs, Germany) with the electrode tips extending 300  $\mu$ m beyond the tip of the optical fibre. An epidural screw electrode (stainless steel,  $\phi$ 1.57 mm, Bilaney Consultants, Germany) was placed contralaterally as ground/reference electrode. After a week of recovery, the recording period was started.

### 2.2.2 Electrophysiology

For EEG recording, the implanted electrodes were referenced to stainless steel microscrew placed on the contralateral side. The electrode leads and optical patch cord were connected to an electro-optical swivel to allow free movement of the animals. These signals were filtered with a 2nd order high pass filter at 0.159 Hz and amplified by a factor of 500 prior to digitisation with a USB-6259 National Instruments Data Acquisition device (NIDAQ) (National Instruments, Austin, Texas, USA) which stored the acquired data locally on a computer for offline analysis. The digitisation had an accuracy of 16-bits over a range of  $\pm 10$  V and thus has a resolution of  $\pm 305$   $\mu$ V, which means the resolution on the original (non-amplified) signals was  $\pm 305$   $\mu$ V / 500 =  $\pm 0.61$   $\mu$ V.

The outgoing signals from the embedded system were digitised by the same USB-6259 National Instruments data acquisition device, namely the amplitude correlation used to detect the seizures and the signal from a General Purpose Input Output (GPIO)-pin, which corresponded to the detection/stimulation action of the microcontroller as shown in Figure 1A. In case of a seizure detection without stimulation, the GPIO-pin was set to high during the detection. In case of stimulation, the GPIO-pin was set to high/low in accordance with the actual stimulation pulses that are given.

The output of the responsive neuromodulation system was a 5 V-pulse which connected to an LED driver (T-Cube™ LED driver, Thorlabs, Germany) via a BNC cable, driving a 470 nm fiber-coupled LED (M470F4 & M470F3, Thorlabs, Germany). This LED was coupled to a rotary joint patch cord ( $\phi$ 400  $\mu$ m, NA 0.39, ceramic ferrule  $\phi$ 1.25 mm, RJPSL4, Thorlabs, Germany), which coupled to the implanted optic fibre cannula with a ceramic sleeve (ADAL1, Thorlabs, Germany). As relatively short pulses were used, the accuracy had to be verified by measuring the optical output power at the ferrule of the patch cord using a photometer (PM400, Thorlabs, Germany) prior to implantation as shown in Figure 3. There was a small delay at the on- and offset of the pulses but the difference between the ideal and actual pulse was small enough to be considered irrelevant for this experiment.

### 2.2.3 Recording Protocol

The animals were attached to the recording set-up non-stop for 6 days to minimise risks associated with disconnecting and reconnecting the animals and the associated risk of inter-day variability caused by a

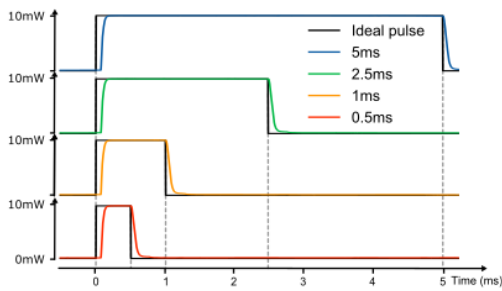


Figure 3: Measurement of optical output power of stimulation pulses of varying duration (0.5, 1, 2.5, 5) ms using T-Cube LED driver and M470F4 LED (Thorlabs, Germany) compared to target pulse.

varying coupling quality. Freedom of movement of the animals was enabled by the use of the rotary patch cord and electrical swivel.

In each stimulation day, a comparison between a maximum of 6 parameters was made with the addition of 2 detection elements for reference. In the IHKA mouse model, animals usually have a seizure rate of 16 seizures/hour (Zeidler et al., 2018). During an 8-hour recording, the occurrence of 160 seizures could be expected which would result in 20 samples of (non-)suppressed seizures for each stimulation element, providing sufficient data to perform the required statistics. After 8 hours of responsive seizure suppression, the system switches to seizure detection only for 16 hours to negate potential long-term effects of the illumination. The elements within a stimulation day occurred in a randomised order to eliminate the potential confounding effects of the stimulation elements on each other. The elements were sampled without repetition to ensure the same rate of occurrence for each element.

For the detection parameters, a detection threshold for the amplitude correlation of 1.11 mV was chosen as a baseline to provide a good balance between detection speed and avoidance of false positives. Reducing the detection threshold avoids false negatives but provides difficulties with analysis as it would be unclear whether the seizure was suppressed or there would not have been a seizure in the first place. The "down" threshold to consider a seizure was finished was set as the detection threshold minus 0.32 mV.

The starting point for the stimulation parameters were based on those indicated in the original WiChR publication by Vierock et al. (Vierock et al., 2022): (1) a wavelength of 473 nm, (2) a pulse frequency of 10 Hz and (3) a pulse duration of 5 ms. For the stimulation power, 10 mW was chosen to ensure sufficient illumination of the hippocampus, as measured at the ferrule of the rotary patch cord. After coupling into the implanted fibre, a loss of 11.6+/-4.1 % was

measured before implantation resulting in a mean output power of 8.8 mW at the tip of the implanted fibre (not accounting for the influence of scar tissue formation due to the implantation). In combination with a maximum duty cycle of 20 %, these settings provide no concern for tissue heating as this would be limited to 1 °C according to simulations by Acharya et al (Acharya et al., 2021). The stimulation duration was fixed at 90 s, corresponding to the 99 % percentile of seizure duration seen in the IHKA mouse model to ensure the entire seizure was suppressed (Zeidler et al., 2018).

The parameters of interest to vary during this study were the pulse frequency and pulse duration as indicated by early parameter explorations and single neuron simulations by Weyn et al. which showed that an increased pulse frequency increases the inhibitory effect while maintaining the duty cycle (Weyn et al., 2024). To study these parameters, a recording protocol was established as illustrated in Figure 4. The first day served to validate the autonomous seizure detection. In the following 4 days, the pulse duration was varied with each detection in the range 1, 2, 3, 4, 5 and 6 ms for four different detection thresholds: 1.11, 1.03, 0.95 and 0.87 mV as the speed of detection was hypothesised to affect the minimal effective pulse duration. For day 2, the highest pulse duration that did not work ( $T_{suppression}$ ) was extracted as the lowest pulse duration resulting in a significant reduction in seizure duration (Welch's t-test,  $p < 0.05$ ) and resulting in a seizure duration reduction of  $\geq 75$  %.

On day 6, both the pulse duration and frequency were varied. The effective pulse duration  $T_{suppression}$  was repeated along with  $T_{suppression}/2$  to validate the (non-)effectiveness. Based on  $T_{suppression}$ , the pulse frequency was multiplied with a factor x2.5 and x5, adjusting the pulse duration to maintain the duty cycle. Finally, an element is tested where the stimulation quantity is reduced after 5 s by decreasing the pulse duration with a factor 1/2 to verify whether the suppressive effect can be maintained with reduced stimulation after the initial suppression. An example of these variations with  $T_{suppression}$  of 5 ms is illustrated in Figure 4.

## 2.2.4 Immunohistochemistry

Immunohistochemistry, a technique using antibodies to visualise proteins in tissue, was performed to analyse the hippocampal structure and the expression of the WiChR opsin. The protocol as previously described, (Desloovere et al., 2021), was followed, with different antibodies to stain for microglia (Iba-1) and RFP (Red Fluorescent Report protein), the tag attached to the WiChR opsin. For Iba-1, rab-

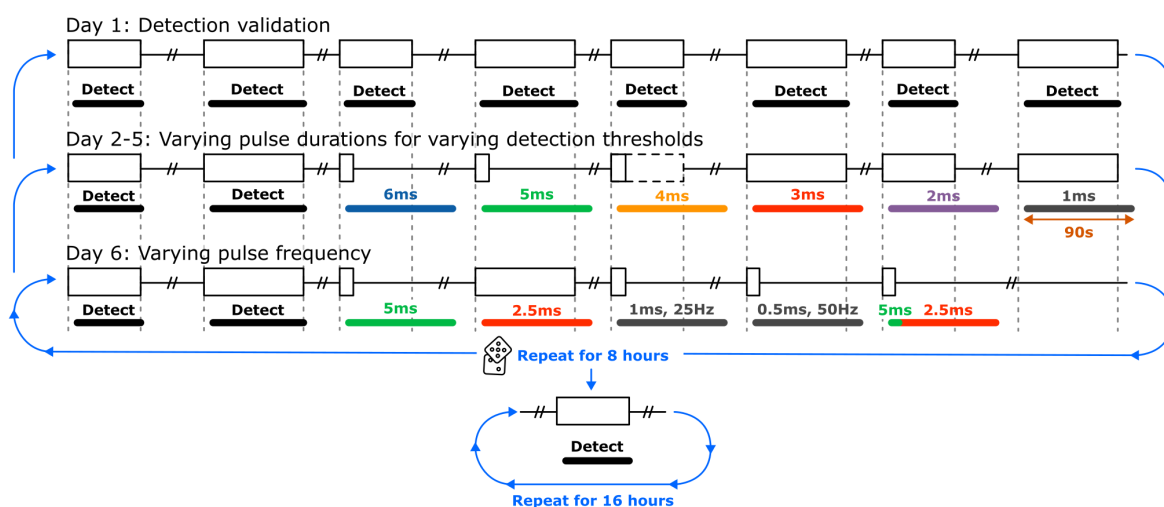


Figure 4: Schematic of recording protocol to evaluate influence of illumination parameters where each block represents a (suppressed) seizure. Unless specified otherwise, illumination is done with a power of 10 mW, a pulse frequency of 10 Hz and a stimulation duration of 90 s. The elements within a day are randomised within each repetition. After 8 hours of responsive stimulation, the protocol switches to detection only for at least 16 hours.

bit anti Iba1 (Abcam Limited, Cambridge, United Kingdom, 1:1000) was used as the primary antibody and goat anti-rabbit 488 nm (Novus Biologicals, Abingdon, United Kingdom, 1:1000) as the secondary antibody. Staining for RFP was performed using chicken anti-RFP (Thermo Fisher Scientific, Massachusetts, United States, 1:1000) as the primary antibody and goat anti-chicken 594 nm as the secondary antibody (Abcam Limited, Cambridge, United Kingdom, 1:1000). Slides were scanned with a fluorescent microscope (Panoramic 250, 3D Histech, 40×magnification) and automatically stitched.

### 2.2.5 Data Analysis

All data was manually annotated in a blind manner (i.e. by only viewing the animal's EEG signals without the signals from the responsive neuromodulation system). A seizure was quantified as repetitive spiking with a minimum spiking frequency of 2 Hz and a minimum duration of 7 s. A seizure was considered finished if followed by a period of 7 s without any spikes. Low frequency spiking activity which generally precedes a seizure was not annotated as part of the seizure. To quantify the detection quality, the manual and automatic annotations obtained from day 1 in the recording protocol (Figure 4) are compared by calculating the percentage of correspondence, the sensitivity and specificity.

Seizures with optogenetic inhibition were annotated as described before if possible with the following considerations: (1) lower amplitude repetitive spiking during the stimulation was considered to be

part of the same seizure as it is an indication that the seizure is only partially suppressed and (2) high frequency spiking activity during stimulation  $\geq 5$  s after the original seizure ended, with duration  $\geq 5$  s were annotated as a new seizure.

For each recording day, there were a number of samples for each set of parameters within that day. These were compared within an animal to verify whether they were significantly different using Welch's t-test ( $p \leq 0.05$  to reject null-hypothesis) as the variances proved unequal according to Levene's variance test ( $p \leq 0.05$ ). To mitigate the influence of the detection speed on the results, the time to detection was subtracted from the seizure duration. As a consequence, the output metric would be more accurately called the "seizure duration after stimulation" but the term "seizure duration" will be used for conciseness.

## 3 RESULTS

Of the initial 12 mice, only 2 showed the spontaneous seizures as expected in the IHKA mouse model, coded SL038 and SL040, and could be used to analyse the seizure detection and consequent optogenetic seizure suppression. This sample size is too small for inter-animal analysis and statistics so all following results remain limited to a comparison within each animal.

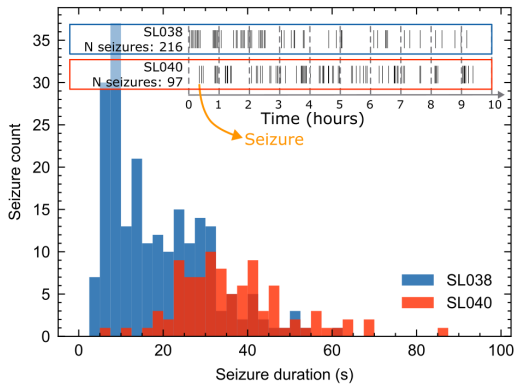


Figure 5: Comparison of seizure characteristics between SL038 and SL040 with histograms of seizure duration and a timeline displaying the occurrence of seizures across the 10 hour recording.

### 3.1 Seizure Detection

Firstly, a comparison was made between the online calculation of the amplitude correlation by the MCU and an offline calculation performed in Python using the same settings for the computation to validate the online calculation by the embedded system. For a 1-hour recording, this showed a correlation between the online and offline correlation with a Pearson  $R^2$  of 97.5 % and a mean error of  $0.82 \mu\text{V}$ , illustrating a strong correspondance between the online and offline calculations.

Table 1 shows the results of the autonomous seizure detection of these two animals. A clear difference can be seen between the two animals under consideration, SL038 and SL040, which can be attributed to a difference observed between the characteristics of the spontaneous seizures as illustrated in Figure 5. SL038 shows a high number of seizures  $>20$  seizures/hour with a relatively short duration. Figure 7A shows a representative EEG-trace with these repetitive occurrences of high frequency spiking activity which fall just around the criteria to be classified as seizures. The seizure detection algorithm was tuned to respond to activity longer than 5 s so encounters difficulties annotating these short seizures with a duration between 5-10 s, leading to a relatively low sensitivity of 42.5 %. Despite this, the seizure detection algorithm achieved an accuracy of 91.3 % and a specificity of 98.0 %.

SL040 displays longer and less frequency spontaneous seizures with an average duration 36.5 s and a rate of almost 10 seizures/hour (Zeidler et al., 2018). These were easier to detect automatically, which is reflected in the increased accuracy (97.8 %), sensitivity (85.8 %) and specificity (99.0 %) compared to SL038. For both animals, the optimisation towards the avoid-

ance of false positives is reflected in a higher specificity compared to the sensitivity.

Table 1: Results of autonomous seizure detection using the amplitude correlation metric and a detection threshold of 1.11 mV.

	SL038	SL040
Nr of seizures	216	97
Mean seizure duration	19.3 s	36.5 s
Standard deviation	$\pm 11.6$ s	$\pm 13.2$ s
Accuracy	91.3 %	97.8 %
Sensitivity	42.5 %	85.8 %
Specificity	98.0 %	99.0 %
Median time to detection	5.4 s	4.0 s

### 3.2 Seizure Suppression

Figure 7A-B shows EEG traces for SL038 and SL040 showing representative examples of spontaneously occurring and suppressed seizures. For SL038, an immediate suppression can be seen without the occurrence of spiking activity during the stimulation period for a pulse duration of 5ms. For SL040, the effect of the illumination does not lead to complete seizure suppression as shown by a comparison of the resulting seizure duration in Figure 6. The reduction in seizure duration for 5ms pulses is 51.6 %, which is below the target of 75 %. Therefore, the protocol in Figure 4 was modified for SL040 to use a pulse duration of 2.5, 5, 7.5, 10, 15 and 20 ms instead of the original 1, 2, 3, 4, 5 and 6 ms. The difference in effect between SL038 and SL040 could be linked to the differences seen in the characteristics of their spontaneous seizures.

Figure 7C-D shows a detailed image of the effect of the illumination on the seizure duration, illus-

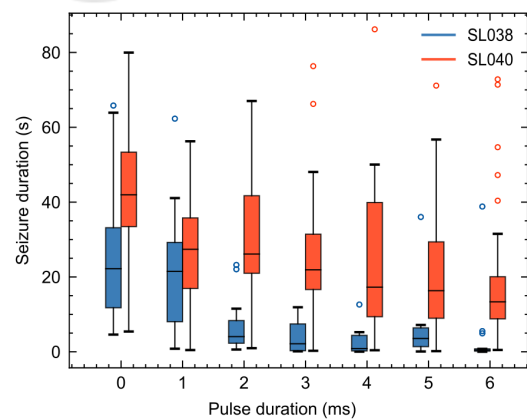


Figure 6: Comparison of resulting seizure duration for a varying stimulation pulse duration between SL038 and SL040.

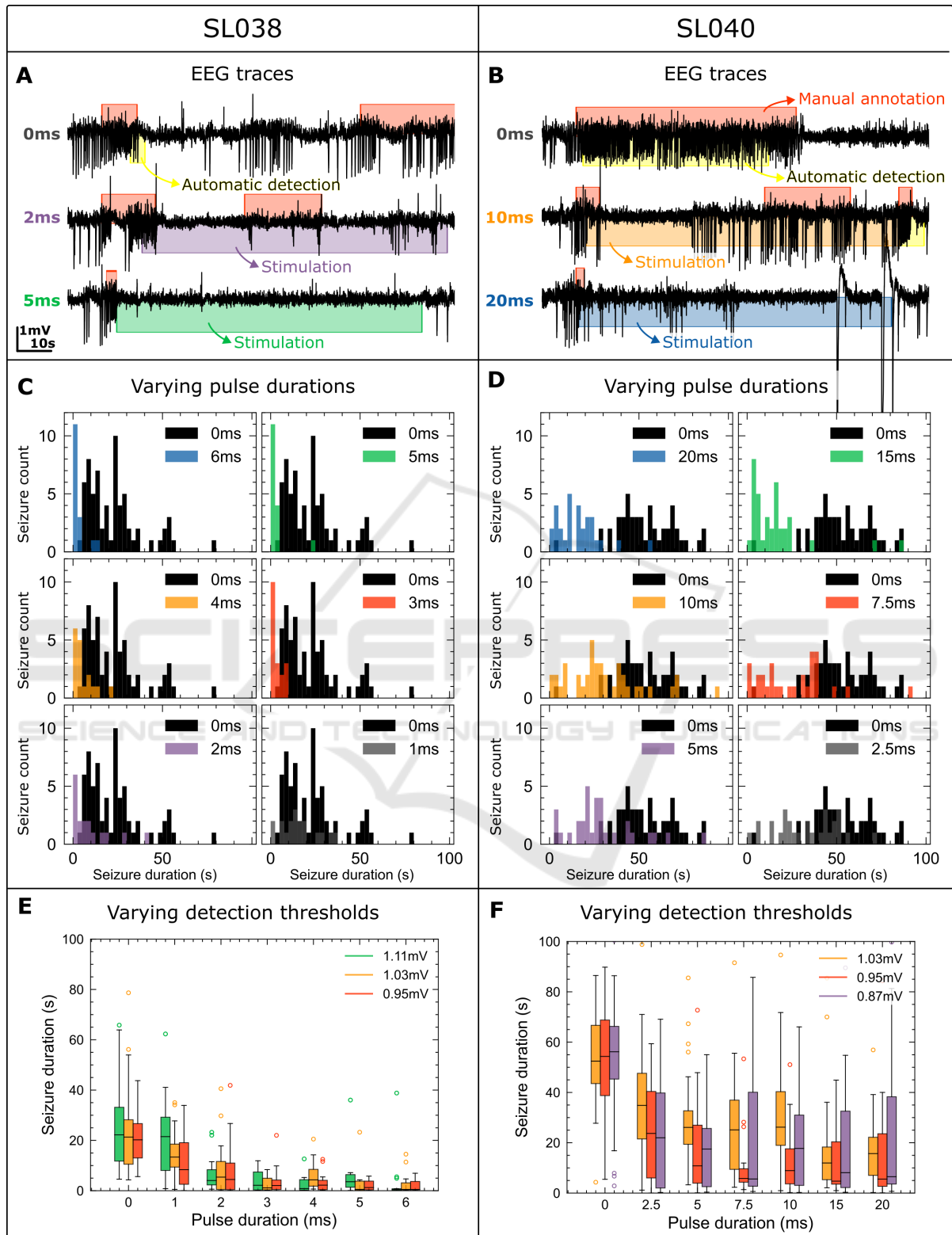


Figure 7: A-B: Typical seizures and effect of 10 Hz illumination with insufficient and sufficient pulse duration for SL038 and SL040. C-D: Histograms of resulting seizure duration for a varying pulse duration for SL038 and SL040. E-F: Box plot of resulting seizure duration for various detection thresholds for SL038 and SL040.

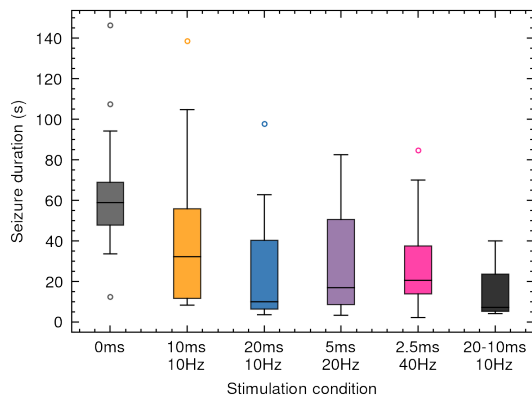


Figure 8: Box plot of reduction in seizure duration for various combinations of pulse duration and frequency for SL040.

trating the inter seizure variability, especially for the shorter pulses and especially for SL040. For SL038, every pulse duration  $\geq 2$ ms has a significant effect ( $p \leq 0.0001$ ) and pulses  $\geq 5$ ms result in a mean resulting seizure duration of 3.5 s, or a reduction of 85.5 % compared to no stimulation which indicates a complete, immediate suppression and was hence selected as the  $T_{suppression}$  pulse duration. The same analysis is performed for SL040 and shows a significant difference between the unstimulated and stimulated seizures ( $p \leq 0.0001$ ) for each pulse duration. However, only a pulse duration  $\geq 15$ ms achieves a reduction in seizure duration  $\geq 70$  % and therefore, 20ms was chosen as  $T_{suppression}$  pulse duration to ensure sufficient suppression.

A comparison of the stimulation effect between the various thresholds can be seen in Figure 7E-F and shows no significant difference in the effect on the seizure between the varying thresholds ( $p > 0.05$ ). A threshold of 1.11 mV is not included in the analysis for SL040 as only 14 seizures occurred during these 8 hours of responsive neuromodulation, resulting in insufficient data quantity for an accurate comparison.

The analysis of stimulation day 6 with varying pulse duration and frequency could only be performed for SL040 due to a loss of signal in SL038, likely cause by a displacement of the depth electrode. For SL040 there is a significant difference between unstimulated and stimulated seizures ( $p \leq 0.05$ ) but no significant difference between the various stimulation settings ( $p > 0.05$ ) as illustrated in Figure 8. This result is questionable however as these results were only obtained for a single animal, which showed a reduced stimulation effect compared to SL038 so this must be considered as an initial observation. Additional data is required from multiple animals to attain a decisive conclusion, especially considering the evident inter-

animal variability in seizure characteristics.

### 3.3 Immunohistochemistry

Of the original 12 mice, only 2 showed spontaneous seizures which is below expectation as the IHKA mouse model is generally very reliable (Zeidler et al., 2018). An explanation had to be found to ensure the safety of the embedded system and this could be found in the results of the immunohistochemistry. Initial analysis of these images shows that from the 10 animals without spontaneous seizures, 4 have either no hippocampal lesion or show very limited degradation of the neuronal cell layers in the dentate gyrus, illustrated in Figure 9A, which explains the lack of spontaneous seizures. The remaining 6 animals showed a severe hippocampal lesion where the injected side was almost entirely degraded as shown in Figure 9B, again providing a different but suitable explanation for the lack of spontaneous seizures. Figure 9C shows the histology of SL040 exhibiting a hippocampal lesion as expected in the IHKA mouse model. None of the histology images showed any indications there might have been an issue with the embedded system, which could be seen as e.g. a cortical lesion caused by an unwanted electrical pulse sent through the electrodes

The inter-animal variability within this experiment could be attributed to a variety of explanations (or a combination thereof) which will be investigated further, including (1) a potential issue with the injec-

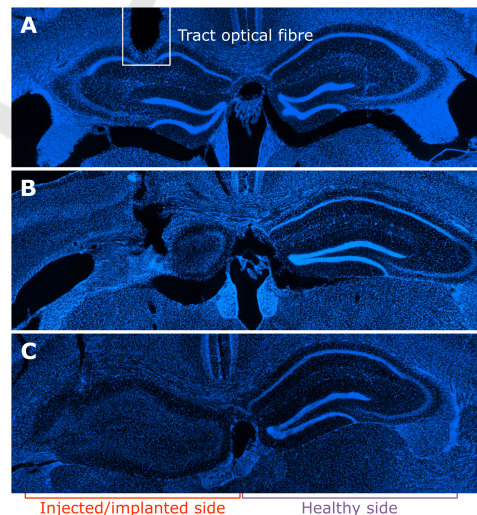


Figure 9: Immunohistochemistry images of DAPI staining in transversal plane around injection/implantation location. A: Example of animal without seizures with minimal hippocampal lesion. B: Example of animal without seizures with major hippocampal damage. C: Example of animal with seizures and typical kainic acid lesion.

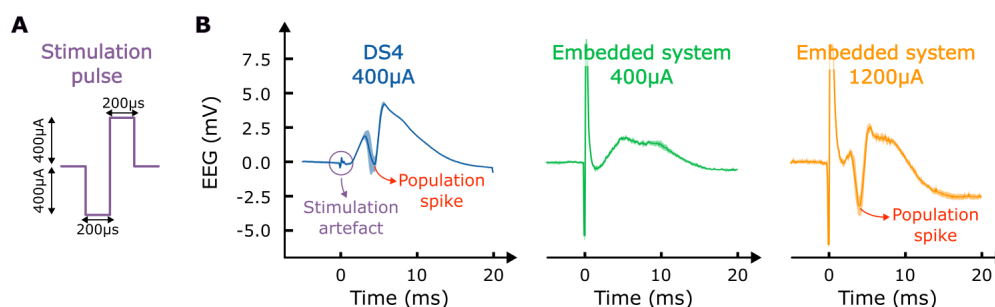


Figure 10: A: Schematic of biphasic current pulse. B: EEG-traces of evoked potentials averaged over 5 repetitions for stimulation pulses generated by the DS4 stimulator (400  $\mu\text{A}$ ) and the embedded system (400 and 1200  $\mu\text{A}$ ).

tion of the kainic acid and/or the WiChR viral vector, (2) potential toxicity due to the combination of the WiChR viral vector and the kainic acid, (3) the relatively high titer of the WiChR viral vector and/or (4) a severe immune response triggered by the implantation of the relatively large optical fibre ( $\phi 400\mu\text{m}$ ). A follow-up study will aim to tackle these potential issues.

### 3.4 Evoked Potentials

A final experiment was conducted with the aim to test the ability of the embedded system to deliver accurate biphasic current pulses to generate evoked potentials for potential use in a responsive neuromodulation experiment based upon brain excitability. The experiment was performed simultaneously with an acute experiment under anaesthesia as described by Spanoghe et al. (Spanoghe et al., 2024). For stimulation, a biphasic current pulse with a phase duration of 200  $\mu\text{s}$  and a current amplitude of  $\pm 400\mu\text{A}$  was generated using the DS4 current stimulator (Digitimer, United Kingdom) as shown in Figure 10A. At the end of the experiment, the DS4 stimulator was replaced by the embedded system to allow a direct comparison. Previous bench top testing showed that both systems provided an identical stimulation pulse over a 10 k $\Omega$  resistor.

However, *in vivo*, there was a difference as the addition of the embedded system in the recording setup introduced noise within the recording, likely due to grounding issues. These experiments were performed under anaesthesia, which forms a less controlled environment for EEG recording compared to the environment for housing and chronic EEG recordings as used in the previously described chronic responsive neuromodulation experiment. As a consequence, the 400  $\mu\text{A}$  pulses from the embedded system were more noisy and resulted in a different evoked potential compared to the DS4 stimulator as shown in Figure 10B for 5 averaged repetitions of this stimula-

tion pulse. The evoked potentials from the embedded system show an increased stimulation artefact and the evoked potential does not contain a population spike, i.e. the negative peak generated by collective generation of action potentials by the neurons. When increasing the stimulation amplitude to 1200  $\mu\text{A}$ , it was possible to generate an evoked potential with a population spike.

## 4 CONCLUSION

The embedded system has been demonstrated to be functional and can be used for responsive neuromodulation experiments using electrical or optical stimulation modalities though more optimisation is needed for the use of biphasic current pulses with a short phase duration. The design of this embedded system shows the feasibility of performing chronic responsive neuromodulation reliably with a minimalist hardware and software design.

The seizure detection algorithm using the amplitude correlation metric is simple yet surprisingly effective. An improvement can be made by the implementation of the use of an adaptive threshold based on the use of a long-term average of the amplitude correlation to mitigate inter-animal variability in signal strength. For the future clinical application however, this type of responsive neuromodulation using seizure detection will be insufficient as you allow the seizure to start before intervening. Ideally, the seizure would be predicted or forecasted and preventive stimulation would be used (Mormann et al., 2007; Baud et al., 2022).

The therapeutic potential of seizure suppression using the WiChR opsin is evident as seen by the quick suppressive effect using only limited stimulation. However, experimental difficulties limited the scope of this study to an analysis of only 2 animals which is insufficient to draw conclusions, especially considering the inter-animal variability which was ev-

ident in this study. Future experiments will aim to increase the number of animals included in the study to allow more thorough analysis and statistics on the seizure suppression and the influence of the stimulation parameters.

## AUTHOR CONTRIBUTIONS

SL - System design, data analysis, writing; LDS, JS, MV, SC - Surgical interventions, animal welfare; JV - Design and supply of WiChR viral vector; RV, RR, PB - Supervision, funding acquisition

## REFERENCES

- Acharya, A. R., Vandekerckhove, B., Larsen, L. E., Delbeke, J., Wadman, W. J., Vonck, K., Carrette, E., Meurs, A., Vanfleteren, J., Boon, P., Missinne, J., and Raedt, R. (2021). In vivo blue light illumination for optogenetic inhibition: effect on local temperature and excitability of the rat hippocampus. *Journal of neural engineering*, 18.
- Baud, M. O., Proix, T., Gregg, N. M., Brinkmann, B. H., Nurse, E. S., Cook, M. J., and Karoly, P. J. (2022). Seizure forecasting: Bifurcations in the long and winding road. *Epilepsia*.
- Craey, E. (2022). A-novel-photocaged-adenosine-a1-receptor-agonist-for-closed-loop-optical-control-of-hippocampal-neurotransmission-and-suppression-of-epileptiform-bursts-in-an-ex-vivo-slice-model-for-epilepsy.
- Craey, E., Hulpia, F., Spanoghe, J., Manzella, S., Larsen, L. E., Sprengers, M., Bundel, D. D., Smolders, I., Carrette, E., Delbeke, J., Vonck, K., Boon, P., Calenbergh, S. V., Wadman, W. J., and Raedt, R. (2022). Ex vivo feedback control of neurotransmission using a photocaged adenosine a1 receptor agonist. *International journal of molecular sciences*, 23.
- Desloovere, J., Boon, P., Larsen, L. E., Goossens, M. G., Delbeke, J., Carrette, E., Wadman, W., Vonck, K., and Raedt, R. (2021). Chemogenetic seizure control with clozapine and the novel ligand jhu37160 outperforms the effects of levetiracetam in the intrahippocampal kainic acid mouse model. *Neurotherapeutics*, 19:342.
- Ebrahim, A. A. and Tungu, A. (2022). Neuromodulation for temporal lobe epilepsy: a scoping review. *Acta Epileptologica*, 4:1–11.
- Instruments, T. T. (2008). An-1515 a comprehensive study of the howland current pump (rev. a) — enhanced reader.
- Krook-Magnuson, E., Armstrong, C., Oijala, M., and Soltesz, I. (2013). On-demand optogenetic control of spontaneous seizures in temporal lobe epilepsy. *Nature Communications* 2013 4:1, 4:1–8.
- Medina, R., Ho, A., Reddy, R., Chen, J., and Castellanos, J. (2023). Narrative review of current neuromodulation modalities for spinal cord injury. *Frontiers in Pain Research*, 4.
- Mormann, F., Andrzejak, R. G., Elger, C. E., and Lehnertz, K. (2007). Seizure prediction: the long and winding road. *Brain : a journal of neurology*, 130:314–333.
- Pederson, D. J., Quinkert, C. J., Arafat, M. A., Somann, J. P., Williams, J. D., Bercich, R. A., Wang, Z., Albers, G. O., Jefferys, J. G., and Irazoqui, P. P. (2019). The bionode. *ACM Transactions on Embedded Computing Systems (TECS)*, 18:400.
- Ryvlin, P. and Jehi, L. E. (2021). Neuromodulation for refractory epilepsy. *Epilepsy currents*, 22:11–17.
- Shon, A., Chu, J. U., Jung, J., Kim, H., and Youn, I. (2017). An implantable wireless neural interface system for simultaneous recording and stimulation of peripheral nerve with a single cuff electrode. *Sensors (Basel, Switzerland)*, 18.
- Spanoghe, J., Boon, P., Vergaelen, M., Colvenaer, M. D., Mariman, T., Vonck, K., Carrette, E., Wadman, W., Craey, E., Larsen, L. E., Sprengers, M., Missinne, J., Calenbergh, S. V., Bundel, D. D., Smolders, I., and Raedt, R. (2024). Photopharmacological activation of adenosine a1 receptor signaling suppresses seizures in a mouse model for temporal lobe epilepsy. *bioRxiv*, page 2024.07.04.602052.
- Vierock, J., Peter, E., Grimm, C., Rozenberg, A., Chen, I. W., Tillert, L., Scalise, A. G. C., Casini, M., Augustin, S., Tanese, D., Forget, B. C., Peyronnet, R., Schneider-Warme, F., Emiliani, V., Bèjà, O., and Hegemann, P. (2022). Wicher, a highly potassium-selective channelrhodopsin for low-light one- and two-photon inhibition of excitable cells. *Science Advances*, 8.
- Weyn, L., Tarnaud, T., Schoeters, R., Becker, X. D., Joseph, W., Raedt, R., and Tanghe, E. (2024). Computational analysis of optogenetic inhibition of ca1 neurons using a data-efficient and interpretable potassium and chloride conducting opsin model. *bioRxiv*, page 2024.10.17.618665.
- White, A. M., Williams, P. A., Ferraro, D. J., Clark, S., Kadam, S. D., Dudek, F. E., and Staley, K. J. (2006). Efficient unsupervised algorithms for the detection of seizures in continuous eeg recordings from rats after brain injury. *Journal of Neuroscience Methods*, 152:255–266.
- Zeidler, Z., Brandt-Fontaine, M., Leintz, C., Krook-Magnuson, C., Netoff, T., and Krook-Magnuson, E. (2018). Targeting the mouse ventral hippocampus in the intrahippocampal kainic acid model of temporal lobe epilepsy. *eNeuro*, 5:ENEURO.0158–18.2018.